

This discussion paper is/has been under review for the journal Ocean Science (OS).
Please refer to the corresponding final paper in OS if available.

On the glacial and inter-glacial thermohaline circulation and the associated transports of heat and freshwater

M. Ballarotta¹, S. Falahat², L. Brodeau², and K. Döös²

¹Department of Physical Geography and Quaternary Geology, Bolin Centre for Climate Research, Stockholm University, 106 91 Stockholm, Sweden

²Department of Meteorology/Oceanography, Bolin Centre for Climate Research, Stockholm University, 106 91 Stockholm, Sweden

Received: 20 February 2014 – Accepted: 12 March 2014 – Published: 20 March 2014

Correspondence to: M. Ballarotta (maxime.ballarotta@natgeo.su.se)

Published by Copernicus Publications on behalf of the European Geosciences Union.

Title Page

Abstract

Introduction

Conclusions

References

Tables

Figures

◀

▶

◀

▶

Back

Close

Full Screen / Esc

Printer-friendly Version

Interactive Discussion



Abstract

The change of the thermohaline circulation (THC) between the Last Glacial Maximum (LGM, ≈ 21 kyr ago) and the present day climate are explored using an Ocean General Circulation Model and stream functions projected in various coordinates. Compared to the present day period, the LGM circulation is reorganised in the Atlantic Ocean, in the Southern Ocean and particularly in the abyssal ocean, mainly due to the different haline stratification. Due to stronger wind stress, the LGM tropical circulation is more vigorous than under modern conditions. Consequently, the maximum tropical transport of heat is slightly larger during the LGM. In the North Atlantic basin, the large sea-ice extent during the LGM constrains the Gulf Stream to propagate in a more zonal direction, reducing the transport of heat towards high latitudes and reorganising the freshwater transport. The LGM circulation is represented as a large intrusion of saline Antarctic Bottom Water into the Northern Hemisphere basins. As a result, the North Atlantic Deep Water is shallower in the LGM simulation. The stream functions in latitude-salinity coordinates and thermohaline coordinates point out the different haline regimes between the glacial and interglacial period, as well as a LGM Conveyor Belt circulation largely driven by enhanced salinity contrast between the Atlantic and the Pacific basin. The thermohaline structure in the LGM simulation is the result of an abyssal circulation that lifts and deviates the Conveyor Belt cell from the area of maximum volumetric distribution, resulting in a ventilated upper layer above a deep stagnant layer, and an Atlantic circulation more isolated from the Pacific. An estimation of the turnover times reveal a deep circulation almost sluggish during the LGM, and a Conveyor Belt cell more vigorous due to the combination of stronger wind stress and shortened circulation route.

Glacial and inter-glacial THC

M. Ballarotta et al.

Title Page

Abstract

Introduction

Conclusions

References

Tables

Figures



Back

Close

Full Screen / Esc

Printer-friendly Version

Interactive Discussion



1 Introduction

The thermohaline circulation (THC) is the large time- and spatial-scales ocean circulation associated with the transports of heat and salt, and is known to control the climate variability (Knight et al., 2005; Zhang et al., 2007). In the North Atlantic region, the THC is characterised by an overturning circulation, the Atlantic Meridional Overturning Circulation (AMOC), which is often used as an indicator for climate change (Letcher, 2009). This AMOC is crucial because, in the present-day climate, it participates in a large amount of the heat transport from the tropics to higher latitudes (Ganachaud and Wunsch, 2000). It also plays an important role in the oceanic uptake of CO₂ (Zickfeld et al., 2008), the ventilation of the deep ocean (Knight et al., 2002; Bryan et al., 2006) and the reorganisation of the passive and active tracers (e.g., temperature, salinity, greenhouse gases, nutrients). It is suggested that the intensity of the AMOC may have been different in the past and might also change in a near future (Manabe and Stouffer, 1994; Rahmstorf, 2002; Schmittner et al., 2005). Similarly, the Southern Ocean is identified as a key region of the climate system. It also participates in the oceanic uptake of heat and carbon dioxide from the atmosphere (Gruber et al., 2009). Moreover, the wind and buoyancy fluxes in this region are the main sources of energy for driving the large scale deep meridional overturning circulation (see e.g., Toggweiler and Samuels, 1998; Marshall and Speer, 2012).

The three dimensional aspect of the THC is however difficult to represent. The schematic representation of the THC has improved since the 19th century (Richardson, 2008). Originally illustrated for the Atlantic basin, since the late 1980s most of the THC representations show the inter-ocean basin exchange of waters, such as, for example the Great Conveyor Belt representation by Broecker (1991). Some representations also emphasise the central role that plays the Southern Ocean for redistributing the waters in the Indo-Pacific and the Atlantic basins. The stream functions are widely used to investigate and represent the ocean circulation. They show the averaged circulation in a two dimensional framework and capture the wind-driven and the thermohaline

Glacial and inter-glacial THC

M. Ballarotta et al.

Title Page

Abstract

Introduction

Conclusions

References

Tables

Figures



Back

Close

Full Screen / Esc

Printer-friendly Version

Interactive Discussion



2 Numerical simulations

The three-dimensional temperature, salinity and velocity fields, used to diagnose the large-scale oceanic circulation, originate from integrations carried out with the ocean general circulation model NEMO (Nucleus for European Modelling of the Ocean, Madec, 2008). This is the ocean component of several coupled earth-system models (Hazeleger et al, 2010; Voldoire et al., 2012; Dufresne et al., 2013) and is used extensively to perform hindcast (Barnier et al., 2007) and forecast (Storkey et al., 2010) simulations. It solves the primitive equations and is run, in our experiments, on its $1^\circ \times 1^\circ$ grid resolution, namely ORCA1. It has 64 vertical levels with a refined mesh near the surface and adaptive bottom boxes (partial-step method) for a better representation of the bathymetry (Barnier et al., 2006). Temperature and salinity are linked to the density via the non-linear equation of state (Jackett and McDougall, 2003). The sub-grid parametrization of horizontal turbulent processes is based on the Gent and McWilliams formulation (Gent and McWilliams, 1990). Hence, an eddy-induced velocity is taken into account in the computation of the stream functions. The ocean model is coupled every two model-hours with the multi-layer thermodynamic-dynamic LIM sea-ice model version 2 (Fichefet and Morales Maqueda, 1997). LIM computes the thermodynamic growth and decay of the sea-ice, as well as its dynamic and transport. It takes into account the sub-grid scale effects of snow and ice thickness.

The two following experiments are designed:

1. A LGM ocean-only simulation forced by a 49 years long atmospheric forcing and an initial state extracted from a coupled experiment by Brandefelt and Otto-Bliesner (2009). This experiment, referred to “LGM_E”, is also described by Ballarotta et al. (2013).
2. A present-day ocean-only hindcast simulation forced by an ERA40-based atmospheric forcing covering 1958 to 2006 (Brodeau et al., 2010). This experiment is referred to as “PD_E”.

OSD

11, 979–1022, 2014

Glacial and inter-glacial THC

M. Ballarotta et al.

Title Page

Abstract

Introduction

Conclusions

References

Tables

Figures

◀

▶

◀

▶

Back

Close

Full Screen / Esc

Printer-friendly Version

Interactive Discussion



Title Page

Abstract

Introduction

Conclusions

References

Tables

Figures

◀

▶

◀

▶

Back

Close

Full Screen / Esc

Printer-friendly Version

Interactive Discussion



NEMO is run for a period of 1000 years by periodically repeating the surface atmospheric forcing set. Our analysis is based on the last 50 years of each experiment. The model has a weak drift after 1000 years (Fig. 1). The globally averaged temperature trends in the upper 1000 m are less than $0.05^{\circ}\text{C}/\text{Century}$ in LGM_E and less than $0.2^{\circ}\text{C}/\text{Century}$ in PD_E . The temperature trends in the deep ocean (below 1000 m) are less than $0.02^{\circ}\text{C}/\text{Century}$ in both runs. The globally averaged salinity trends are weak (less than $0.02 \text{ PSU}/\text{Century}$).

3 Results

In this section, the different aspects of the large-scale circulation in LGM_E and PD_E are analysed using stream functions projected in various coordinate frameworks. The results are firstly presented in geographical coordinates, serving to understand the circulation in thermohaline coordinates. The maximum of the overturning cells is summarised in Table 1. The mathematical formulations for each type of stream function are presented in the Appendix.

3.1 Transports in geographical coordinates

3.1.1 Tropical circulation

The tropical cells in LGM_E and PD_E are similar in extent. They are mainly associated with the Indo-Pacific circulation (Figs. 4e and f, 5e and f, 6e and f and 7e and f). They transform the warm surface equatorial waters in the upper 500 m of the ocean into colder (about 13°C in PD_E , 6°C in LGM_E) mid-latitude waters. These waters return subsequently equatorward in increasing their heat content. Due to the cold atmospheric condition, the tropical cells in LGM_E are slightly shifted towards colder temperatures than in PD_E (Fig. 6e and f). The maximum volume transport within these cells are similar or slightly larger in LGM_E than in PD_E (Table 1), due to the stronger wind stress in LGM_E (Figs. 2 and 3). Similarly, the Pacific circulation related to the tropical gyres is

about 20 Sv stronger in LGM_E than in PD_E (Figs. 2 and 3). As a results, the maximum poleward heat transports near 18° N and S are slightly larger in LGM_E (1.5 PW at 18° S and 1 PW at 18° N). In PD_E, the cells reorganise the saltiest water of the Indo-Pacific basin (Fig. 4f). In LGM_E, the saltiest water are found in the deep ocean (Fig. 4e). The associated freshwater transport is dominantly directed southwards and the maximum transports are at 10° S and 34° N. Between 40° S and 20° S, the northward transport of freshwater from the Southern Ocean is larger in PD_E (0.5 Sv) than in LGM_E, due to a larger amount of melting sea-ice in PD_E.

3.1.2 Atlantic Ocean circulation

The Northern Hemisphere tropical cell is embedded into a meridional large cell mainly associated with the NADW (Figs. 4c and d, 5c and d and 6c and d). This latter cell is shallower in LGM_E than in PD_E, respectively near 1500 m in LGM_E as shown in Fig. 4c, near 2500 m in PD_E as shown in Fig. 4d. Due to the important zonal component associated to the Gulf Stream and the large sea-ice extent, the zonal component of the North Atlantic gyre is dominant in LGM_E (Figs. 2 and 3) and the maximum of the AMOC is shifted southward compared to PD_E. When taken below 500 m, this maximum in PD_E and LGM_E is 13 Sv in latitude-depth coordinates. In the other coordinates, the maximum of the AMOC is larger in PD_E than in LGM_E (cf., Table 1). Associated with this AMOC, a large amount of saline water fills the deep ocean between 20 and 40° N in LGM_E. The AMOC cell transports the mid-latitude warm and saline waters towards higher latitude, where they become denser (colder) as shown in Figs 5c and d (Fig. 6c and d). Near 60° N, the waters are transported southward with a near isopycnal (isothermal and isohaline) transformation and they exit the Atlantic basin near 40° S. Between the Equator and 40° N, the transport of heat in the Atlantic basin is slightly higher in LGM_E than in PD_E, because the volume transport in LGM_E is stronger in the NADW and the transport in the AABW is weak. Between 40° N and 90° N, the meridional heat transport in LGM_E is smaller due to the large sea-ice extent which constrains the Gulf Stream warm current into a more zonal propagation. In latitude-salinity

Title Page

Abstract

Introduction

Conclusions

References

Tables

Figures

◀

▶

◀

▶

Back

Close

Full Screen / Esc

Printer-friendly Version

Interactive Discussion



Title Page

Abstract

Introduction

Conclusions

References

Tables

Figures

◀

▶

◀

▶

Back

Close

Full Screen / Esc

Printer-friendly Version

Interactive Discussion



coordinates, the main differences between LGM_E and PD_E are in the Atlantic basin (Fig. 7c and d). In LGM_E , a large intrusion of saline water originating from the Southern Ocean takes place between $40^\circ S$ and $20^\circ N$. This intrusion squeezes and isolates the North Atlantic circulation from the southern part of the Atlantic basin. Consequently, the freshwater transport in LGM_E is affected by these changes. Between $20^\circ N$ and $90^\circ N$, it is directed southward in PD_E , representing the transfer of freshwater from the pole to the mid-latitudes. In LGM_E , the freshwater transport is directed northward between $47^\circ N$ and the pole, southward between $20^\circ N$ and $47^\circ N$. This corresponds to the transfers of the mid-latitude freshwater (due to melting sea-ice) by the North-Atlantic and sub-polar gyres. Between $37^\circ S$ and $20^\circ N$, the freshwater transport in LGM_E is directed northward associated with the waters originating from the south pole.

3.1.3 Southern Ocean and deep circulations

The Deacon Cell is found in a region with important tilting of the isopycnal layers (isotherm and isohaline as shown in Fig. 4a and b). Compared to PD_E , the structure of the Southern Ocean zonally averaged temperature and salinity in LGM_E is shifted equatorward due to the larger sea-ice extent. Moreover, the deep ocean in LGM_E is essentially filled with cold and saline waters which originate from Southern Ocean surface. The zonally-averaged isopycnal layers in LGM_E are hence slightly shifted equatorward and most of them are concentrated in a thinner surface layer than in PD_E . Therefore, the Deacon Cell is located between $58^\circ S$ and $40^\circ S$ in LGM_E and penetrates about 1000 m deep whereas it is between $65^\circ S$ and $38^\circ S$ and reaches about 4000 m in PD_E . In latitude-density (Fig. 5a and b) and latitude-temperature coordinates (Fig. 6a and b), the maximum overturning in the Deacon Cell is reduced compared to the averaging in latitude-depth coordinates. In latitude-salinity coordinates, the Southern Ocean maximum overturning (Fig. 7a and b) has the same order of magnitude than in latitude-depth coordinates.

The AABW in PD_E is homogenous both in temperature and salinity (Fig. 4b and h). It is cold (-2 to $2^\circ C$) and relatively fresh (34.5 to 35 PSU). The associated circulation

Title Page

Abstract

Introduction

Conclusions

References

Tables

Figures

◀

▶

◀

▶

Back

Close

Full Screen / Esc

Printer-friendly Version

Interactive Discussion



exports the coldest Southern Ocean surface water down to a depth of 2000 m. The AABW in LGM_E is relatively homogenous in temperature and the salinity ranges from 35.5 to 37 PSU (Fig. 4a and g). As a result, the abyssal waters are denser in the LGM_E than in PD_E, and a clear overturning cell appears in latitude-density coordinates for LGM_E (Fig. 5a), capturing a deep ocean stratification. In PD_E, the abyssal MOC is nearly along the 28.1 kgm⁻³ neutral density surface because the abyssal ocean is homogenous in density. The MOC associated to the AABW consists in a near isothermal transformation of the coldest waters in latitude-temperature coordinates. The abyssal circulation in the Atlantic Ocean in LGM_E is extremely weak in temperature coordinate due to weak thermal stratification below 1000 m. In latitude-temperature, a closed circulation centred near 50° S in LGM_E and 60° S in PD_E is associated with the surface overturning (Fig. 6a and b). In this region, the transports of heat in LGM_E and PD_E are similar (about 0.5 PW) and directed towards Antarctica. The deep MOC in LGM_E are also characterised by a circulation of saline waters ranging from 36 to 37 PSU, which maintain a maximum MOC of 6 Sv near 60° S. Associated with this overturning about 0.3 Sv of freshwater are transported towards Antarctica. In latitude-depth coordinates, the maximum MOC in the AABW is stronger in LGM_E (19 Sv) than in the PD_E (8 Sv). A deep clockwise circulation, located 4000 m deep and between 40° S and the equator, is present in the Indo-Pacific basin and may be the result of slight meridional density gradient which is able to sustain a clockwise circulation. When the circulation associated with the AABW is projected in the other coordinates, the maximum overturning is smaller in LGM_E than in PD_E and the deep clockwise circulation vanishes which suggest that this feature might also be linked to the averaging in z-coordinates.

3.2 Transports in thermohaline coordinates

This section presents the THC in thermohaline coordinates, the volumetric distribution in the θ -S diagram and an estimation of the time scale of the circulation.

3.2.1 Thermohaline stream function and transport of heat/freshwater in temperature and salinity coordinates

The ocean circulation in thermohaline coordinates consists of three main cells (Figs. 8 and 9): (1) a tropical cell, which reflects the water mass transformation in the upper near-equatorial Pacific; (2) a Conveyor Belt cell, which is the dominant circulation in the diagram and captures the inter-ocean transport of heat and salt; and (3) a low temperature cell which reflects to the AABW. This latter cell is particularly strong in LGM_E due to the important saline stratification in the abyss (Fig. 8). In PD_E, this cell is small (centred at 34.7 PSU and 1 °C) because the modern deep ocean is relatively homogenous in temperature and salinity (Fig. 9). Hence, the low temperature cell in PD_E does not participate significantly in the global transport of heat and freshwater. On the contrary, the freshwater transport associated with the low temperature cell in LGM_E reaches a maximum of about 0.4 Sv in the -2 °C isotherm.

The tropical cell in PD_E is centred at 35 PSU -27 °C and has a maximum transport of 21 Sv. It corresponds to the shallow wind-driven transport (equatorial undercurrent in the central Pacific). It converts the 33.5 to 35 PSU water-masses into saltier (35 to 37 PSU) water-masses (or the 21 to 27 °C water-masses into warmer 27 to 30 °C water-masses). The tropical cell in LGM_E is shifted towards colder isotherms and fresher isohalines due to the cold condition and the reduced evaporation at the surface. It is hence centred at 34.5 PSU and 24 °C and has a maximum transport of 24 Sv. It converts the 31 PSU to 34.5 PSU water-masses into saltier (34.5 to 35.5 PSU) water-masses (or the 16 to 24 °C water-masses into warmer 24 to 28 °C water-masses). The conversion is nearly isohaline along 34.6 PSU and almost isothermal near 27 °C corresponding to the water-masses transformation at the surface of the western Pacific pool. The maximum heat transport carried by the tropical cell is 0.5 PW in LGM_E. In PD_E, the maximum transport of heat is two times smaller than in LGM_E. The maximum freshwater transports are rather similar between PD_E and LGM_E. The tropical cell transports about 1 Sv near the 25 °C isotherm in LGM_E and near the 28 °C in PD_E.

Title Page

Abstract

Introduction

Conclusions

References

Tables

Figures

◀

▶

◀

▶

Back

Close

Full Screen / Esc

Printer-friendly Version

Interactive Discussion



**Glacial and
inter-glacial THC**

M. Ballarotta et al.

Title Page

Abstract

Introduction

Conclusions

References

Tables

Figures

I◀

▶I

◀

▶

Back

Close

Full Screen / Esc

Printer-friendly Version

Interactive Discussion



The large-scale transport in Conveyor Belt cell (for example the transport between the -2 and -6 Sv streamlines in Figs. 8 and 9) is similar to the Broecker (1991) loop and can be described as follows: the Indo-Pacific surface-waters ($16^{\circ}\text{C} \leq \theta \leq 22^{\circ}\text{C}$ and $34.5 \text{ PSU} \leq S \leq 35 \text{ PSU}$) become colder approaching the Cape Agulhas and enter in the South Atlantic basin ($S \approx 35 \text{ PSU}$). These waters flow northward and increase their salinity and temperature. They cool down near 36.5 – 37 PSU , become fresher (between $\sigma_0 = 28 \text{ kg m}^{-3}$ and $\sigma_0 = 29 \text{ kg m}^{-3}$ in LGM_E , and between $\sigma_0 = 27 \text{ kg m}^{-3}$ and $\sigma_0 = 28 \text{ kg m}^{-3}$ in PD_E) and sink in the deep-ocean to finally upwell in the North Pacific basin as cold and fresh water-masses. Smaller scale transformations exist in the Indo-Pacific and Southern Oceans. For instance, the maximum volume transport in LGM_E takes place near the 34.1 PSU isohaline and is about 20.2 Sv . In PD_E , the volume transport is maximum near the 34.7 PSU with a magnitude of 23.6 Sv . These circulations are associated with the intense transports in the Antarctic Circumpolar Current and the formation of the Antarctic Intermediate Water. The shape of the Conveyor Belt cell is different between the two experiments. In LGM_E , the Conveyor Belt cell occupies more isohaline layers than in PD_E since the Atlantic thermohaline regime is changed. A near-isothermal transformation (near 22°C) appears in the Atlantic basin. It corresponds to the inter-tropical surface circulation driven by the strong salinity contrast between the North and South Atlantic basins in LGM_E (Fig. 4c). This is not observed in PD_E which is mainly driven by a difference in temperature rather than the difference in salinity (Fig. 9). These reorganisations modify the transports of heat and freshwater. In PD_E , a maximum freshwater transport of 1 Sv is found in the 14 – 16°C isotherms and the maximum heat transport (about 1 PW) is in the 34 PSU and 35.5 PSU isohaline (associated with the Indo-Pacific and Atlantic basins heat transports). In LGM_E , the Conveyor Belt cell carries a maximum of 1.2 Sv of freshwater in the 4°C isotherm and the heat transport is more spread between the 35 and 37 PSU isohalines.

3.2.2 Volumetric distribution in the T-S diagram

The different thermohaline regimes between the two periods can be illustrated by projecting the sea-water volumetric distribution in the temperature-salinity coordinates (Figs. 10 and 11). In LGM_E, the maximum volume of sea-water (in $10^{17} \text{m}^3 \text{C}^{-1} \text{PSU}^{-1}$) is made of relatively cold and saline waters. The temperatures are between -2°C and 0°C , and the salinities vary between 36.5 PSU and 37.5 PSU. For the intermediate waters (i.e., between 2°C and 16°C), the important volume of sea-water (more than $10^{14} \text{m}^3 \text{C}^{-1} \text{PSU}^{-1}$) is found in two “branches”: the waters with salinity between 36 PSU and 37 PSU associated with the Atlantic waters; and the relatively fresher waters between 34 PSU and 36 PSU, corresponding to the Indo-Pacific waters (cf. Supplement and Fig. 7). These two branches are not as distinct in PD_E, suggesting that the Atlantic and the Indo-Pacific basins have a closer thermohaline structure under the present-day conditions than for the LGM period. Contrary to PD_E, the Conveyor Belt cell in LGM_E becomes less connected to the deep ocean. This is due to an abyssal circulation which tends to lift and deviate the Conveyor Belt cell from the area of maximum volumetric distribution.

3.2.3 Turnover times

For each simulation, the shortest turnover times (see Appendix A3.2) are found in the tropical cell (Figs. 12 and 13). The stretch of times in the cells can largely differ between two successive layers because of the different length of the circuit in the layers. In PD_E, the turnover times in the Conveyor Belt cell vary between 50 years (where the water conversion is minimum) and more than 2500 years (for the global-scale transports). In LGM_E, the times in the Conveyor Belt cell are shorter (between 50 and 800 years). In the cell representative of the AABW, the times are between 50 and 1000 years in LGM_E, representing the rapid sinking of the water near the surface and the large-scale slow motions in the abyss. In PD_E, the turnover time for the circulation in the AABW is around 50 years corresponding to the rapid sink of the surface circulation near Antarctica. The

Title Page

Abstract

Introduction

Conclusions

References

Tables

Figures

◀

▶

◀

▶

Back

Close

Full Screen / Esc

Printer-friendly Version

Interactive Discussion



Glacial and inter-glacial THC

M. Ballarotta et al.

Title Page

Abstract

Introduction

Conclusions

References

Tables

Figures

◀

▶

◀

▶

Back

Close

Full Screen / Esc

Printer-friendly Version

Interactive Discussion



from the formation of dense waters in the Southern Ocean that fill the North Atlantic and North Pacific basins, and the difference of bathymetry which prevents the redistribution of the waters between the northern and southern basins in some narrow passages. As a results, homogenous dense waters are found in the Northern Hemisphere deep basins preventing density gradient to maintain the deep overturning.

The choice of the coordinate system to project the stream functions is important for the computation and comparison of the maximum overturning and thus the estimation of the transport of heat and freshwater. For example, the maximum overturning in the Deacon Cell is smaller in latitude-density and latitude-temperature coordinates than in latitude-depth coordinates. This is due to both the large eddy-induced velocities (transient eddies) in this region and the choice of an isopycnal framework (Drijfhout, 2005). The maximum AMOC in PD_E and LGM_E is similar in latitude-depth coordinate. It is larger in PD_E than in LGM_E when the calculation is performed in latitude-density, latitude-temperature and latitude-salinity coordinates. This raise the question to know which coordinate framework is the best to estimate the AMOC. In Zhang (2007) and Grist et al. (2012), better estimate of the present-day AMOC is obtained in density coordinate than in depth coordinate. Hence, this reinforces the necessity of investigating the THC in latitude-density coordinate rather than in latitude-depth coordinate. The interpretation of the circulation in latitude-salinity coordinate is more complex. However, by using this latter coordinates system, it is possible to distinguish basin scale transformations and to identify the different haline structure between LGM_E and PD_E . Moreover, in many areas, the three-dimensional structure of the circulation is essential, particularly for the Southern Ocean circulation (Sloyan and Rintoul, 2001; Drijfhout et al., 2003). The thermohaline stream function, which take into consideration the three-dimensional aspect of the circulation, is therefore relevant for capturing the entire Southern Ocean dynamics.

The different thermohaline responses among the paleo-climate models can also be attributable to the choice of the ocean initial state and the length of the model integration. As pointed out by Zhang et al. (2013), the CCSM3 and HadI2 ocean models are

Glacial and inter-glacial THC

M. Ballarotta et al.

Title Page

Abstract

Introduction

Conclusions

References

Tables

Figures

◀

▶

◀

▶

Back

Close

Full Screen / Esc

Printer-friendly Version

Interactive Discussion



initialised with a glacial state. These models simulate a weak AMOC and a high saline stratification in the deep ocean, as observed in LGM_E. The simulated sea-ice extent can also contribute to different thermohaline structure. Otto-Bliesner et al. (2007) and Zhang et al. (2013) point out the important role of sea-ice in the water mass formation. Its impact on the thermohaline regime is identified, for instance, as a factor favouring the densification of the Southern Ocean water in the CCSM3 model (Otto-Bliesner et al., 2007; Brandefelt and Otto-Bliesner, 2009). Similarly, the large sea-ice extent in LGM_E can maintain an expanded and dense AABW coexisting with a shallow NADW, and a reduced ventilation of the deep ocean resulting in large turnover time. A shallowed and weakened AMOC, and an intensified AABW is also found in the models of Butzin et al. (2005) and Hesse et al. (2011), which include an enhanced northward sea-ice export in the Southern Ocean. This leads to the best agreement for capturing the general ¹³C distribution (i.e., water masses geometry) derived from sediment analysis.

Paleo-proxy data also propose various geometries for the LGM ocean state. Paleoproxy reconstructions agree on a shallower NADW and a larger intrusion of the AABW in the North Atlantic during the LGM (Marchitto and Broecker, 2006; Evans and Hall, 2008; Lippold et al., 2012). It is suggested that the interface between the NADW and the AABW is substantially shallower during the LGM than today. This transition depth between the NADW and the AABW is estimated around 1750 m in Tagliabue et al. (2008), which is very close to the value found in LGM_E (near 1500 m). However, their estimation of the maximum AMOC transport (5 Sv) is weaker than in LGM_E (Table 1). Paleoproxy reconstructions based on ²³¹Pa/²³⁰Th ratios suggest that the deep circulation during the LGM is stronger or comparable in strength with present-day transports (Yu et al., 1996; Lynch-Stieglitz et al., 2007; Gherardi et al., 2009; Lippold et al., 2012). Other reconstructions based on oxygen-isotope ratios of benthic foraminifera and δ¹³C data propose that the water renewal in the deep ocean is much slower than today (Lynch-Stieglitz et al., 1999; Hesse et al., 2011). In Tagliabue et al. (2008), the transport associated with the AABW is around 4 Sv whereas it is close to 2 Sv in LGM_E (cf. Table 1). There is also evidence that the deep ocean is homogenous in temperature

during the LGM (near freezing point in Adkins and Schrag, 2001 and between 2 and 4°C colder than today in Martin et al., 2002). Reconstructions of the abyssal salinity also suggest that the deep ocean is filled with the most saline waters and that salinity gradient is the main driver of the LGM abyssal circulation (Adkins et al., 2002). The CCSM3 and HadI2 models (initialised with glacial state) simulate the high salinity in the deep ocean as it is proposed by Adkins et al. (2002). LGM_E also captures the signature of a cold and extremely saline deep ocean. This might be the consequence of a glacial initial state and the large sea-ice extent which contributes to enhance the formation of saline AABW.

5 Conclusions

There is clear evidence that the ocean is more saline during the LGM than during the present-day period due to the large volume of water sequestered in the continental ice sheets during the glacial period. This substantial change, associated with the larger sea-ice extent during the glacial period, modifies the structure of the ocean. The main differences between the LGM and the present-day are found in the Atlantic basin, the Southern Ocean and in the abyss. In comparison to the present-day, the mean thermocline depth is shallower during the LGM. Below this thermocline, the ocean is filled with the most saline waters originating from the Southern Ocean. Near the surface, the volume transports are similar or slightly larger in the tropical cells due to the larger surface wind stress. Consequently, the maximum transport of heat in the tropics is also larger. The AMOC is shallower and the Gulf Stream has a more zonal propagation, reducing the heat transport in high-latitudes. Depending on the choice of coordinates framework, the maximum AMOC during the LGM is either similar or slightly weaker than today. The circulation in the AABW cell is more vigorous in the Southern Ocean and occupies more volume than under present-day condition. In the North Pacific and North Atlantic basins, the deep circulation is almost sluggish due to the weak density meridional gradient. The circulations in latitude-salinity and thermohaline coordinates

Title Page

Abstract

Introduction

Conclusions

References

Tables

Figures

◀

▶

◀

▶

Back

Close

Full Screen / Esc

Printer-friendly Version

Interactive Discussion



Glacial and inter-glacial THC

M. Ballarotta et al.

Title Page

Abstract

Introduction

Conclusions

References

Tables

Figures

◀

▶

◀

▶

Back

Close

Full Screen / Esc

Printer-friendly Version

Interactive Discussion



illustrate the different haline regimes between the LGM and the present-day periods. They also point out the Atlantic and Southern oceans as the regions of important reorganisations. The thermohaline structure in LGM_E is represented by an abyssal circulation which lift and deviate the Conveyor Belt cell from the area of maximum volumetric distribution, resulting in a ventilated upper layer above a deep stagnant layer, and an Atlantic circulation more isolated from the Pacific. The turnover time within the Conveyor Belt cell is shorter during the LGM than today. This shorter travel time in the Conveyor Belt can be explained by the combination of the vigorous surface circulation for the LGM, the shorter route of the near surface circulation and a circulation associated with the AABW that squeezes most of the Conveyor Belt cell in a shallower part of the ocean. The turnover time of the glacial abyssal circulation is large suggesting a near sluggish circulation.

Appendix A

Mathematical formulation of the stream functions

A1 Transport in geographical coordinates

Barotropic stream function

The barotropic stream function is the vertically integrated volume transport at a given location (Eq. A1). It yields the averaged circulation in the horizontal plane.

$$\Psi(x, y) = \int_{x_E}^x \int_{-H}^{\eta} (V + V_{\text{eddy}}) dz dx \quad (\text{A1})$$

Here x is the longitude, y is the latitude, x_E the eastern boundary, H the depth of the water column, η the sea surface elevation, $V + V_{\text{eddy}}$ the meridional velocity including the eddy-induced velocity contribution.

The barotropic stream functions consist in basins scale gyres (Figs. 2 and 3). The volume transport is more vigorous in LGM_E than in PD_E, due to the larger wind-stress acting on the ocean surface during the glacial period (cf. zonally-averaged zonal and meridional wind-stress over the ocean, respectively in Figs. 2–4).

A2 Meridional overturning circulation in depth coordinate

The meridional overturning circulation as a function of depth is, at a given latitude, the volume transports in the water column (Eq. A2).

$$\Psi(y, z) = \int_{x_E}^{x_W} \int_{-H}^z (V + V_{\text{eddy}}) dz dx \quad (\text{A2})$$

Here y is the latitude, z the depth, x_E and x_W the eastern and western boundaries, H the depth of the water column, $V + V_{\text{eddy}}$ the meridional velocity plus the eddy-induced velocity.

The MOC in latitude-depth coordinates in LGM_E and PD_E are shown in Fig. 4 for the Global Ocean, the Atlantic Ocean and the Indo-Pacific basin. The thick-lined contours indicate a clockwise circulation while dash-lines indicate an anti-clockwise circulation. In order to visualise the thermohaline structure for LGM_E and PD_E, the temporally- and zonally-averaged temperature and salinity fields are shown in each figure. The temporally- and zonally-averaged temperature in the Atlantic and the Indo-Pacific basins is documented in the Supplement because the patterns are similar to those found for the global ocean.

In latitude-depth coordinates, the MOC consists mainly of: (1) two near-surface inter-tropical cells; (2) an intermediate cell representative of the North Atlantic Deep Water (NADW) between 40° S and 80° N; (3) a Southern Ocean cell between 40° S and 60° S,

Title Page

Abstract

Introduction

Conclusions

References

Tables

Figures

◀

▶

◀

▶

Back

Close

Full Screen / Esc

Printer-friendly Version

Interactive Discussion



known as the Deacon Cell and (4) a deep ocean circulation related to the Antarctica Bottom Water (AABW).

A2.1 Meridional overturning circulation in density coordinate

The meridional overturning circulation as a function of density is, at a given latitude, the volume transport within the isopycnal (Eq. A3).

$$\Psi(y, \gamma) = \int_{x_E}^{x_W} \int_{z(\gamma)}^{\eta} (V + V_{\text{eddy}}) dz dx \quad (\text{A3})$$

Here y is the latitude, γ the neutral density, $z(\gamma)$ the depth of the neutral density surface, η the sea surface elevation, x_E and x_W the eastern and western boundaries, $V + V_{\text{eddy}}$ the meridional velocity including the eddy-induced velocity contribution.

The MOC in latitude-density coordinates in LGM_E and PD_E are shown in Fig. 5 for the Global Ocean, the Atlantic Ocean and the Indo-Pacific basin. The global MOC in latitude-density coordinates consists of: (1) two opposite tropical cells between 40° S and 40° N, (2) a cell of intermediate waters and (3) a cell of dense waters originating from the Southern Ocean surface.

A2.2 Meridional overturning circulation in temperature coordinate and the transport of heat

The meridional overturning circulation as a function of temperature is, at a given latitude, the volume transport within the isotherms (Eq. A4).

$$\Psi(y, \theta) = \int_{x_E}^{x_W} \int_{\theta_{\min}}^{\theta} (V + V_{\text{eddy}}) d\theta dx \quad (\text{A4})$$

Title Page

Abstract

Introduction

Conclusions

References

Tables

Figures

◀

▶

◀

▶

Back

Close

Full Screen / Esc

Printer-friendly Version

Interactive Discussion



Title Page

Abstract

Introduction

Conclusions

References

Tables

Figures

◀

▶

◀

▶

Back

Close

Full Screen / Esc

Printer-friendly Version

Interactive Discussion



Here y is the latitude, θ the temperature, x_E and x_W the eastern and western boundaries, θ_{\min} the minimum temperature considered, $V + V_{\text{eddy}}$ the meridional velocity plus the eddy-induced velocity.

The integral of the transports along each isotherms at a given latitude is an estimation of the advective meridional heat transport (Eq. A5). A positive heat transport is a transport towards the north pole, a negative transport is towards the south pole.

$$\mathcal{H}(y) = \int_{\theta_{\min}}^{\theta_{\max}} \rho C_p \Psi(y, \theta) d\theta \quad (\text{A5})$$

Here y is the latitude, θ the temperature, $\rho = 1035 \text{ kg m}^{-3}$ the average density of seawater and $C_p \approx 4000 \text{ J (kg }^\circ\text{C)}^{-1}$ the specific heat for seawater.

The MOC in latitude-temperature coordinates in LGM_E and PD_E are shown in Fig. 6 for the Global Ocean, the Atlantic Ocean and the Indo-Pacific basin. The global MOC consists of: (1) two opposite tropical cells between 40° S and 40° N, (2) a cell of intermediate waters and (3) a cell of cold waters originating from the Southern Ocean surface.

A2.3 Meridional overturning circulation in salinity coordinate and the transport of freshwater

The meridional overturning circulation as a function of salinity is, at a given latitude, the volume transport within isohalines (Eq. A6).

$$\Psi(y, S) = \int_{x_E}^{x_W} \int_{S_{\min}}^S (V + V_{\text{eddy}}) dS dx \quad (\text{A6})$$

Here y is the latitude, S the salinity, x_E and x_W the eastern and western boundaries, S_{\min} the minimum salinity considered, $V + V_{\text{eddy}}$ the meridional velocity plus the eddy-induced velocity.

The integral of the transports along each isohaline at a given latitude is an estimation of the meridional freshwater transport (Eq. A7). The positive and negative freshwater transport is a transport towards the north pole and towards the south pole, respectively.

$$\mathcal{F}(y) = \int_{S_{\min}}^{S_{\max}} \frac{\Psi(y, S)}{S_r} dS \quad (\text{A7})$$

Here y is the latitude, S the salinity, and $S_r = 35$ PSU is a constant reference salinity.

The MOC in latitude-salinity coordinates and the associated transports of freshwater are particularly different between LGM_E and PD_E because of the differences in the haline regimes (Fig. 7a and b). The global MOC in latitude-salinity coordinates in PD_E consists of: (1) an anti-clockwise circulation between 80° S and 20° S linking the Southern Ocean waters with the south tropical waters; (2) a clockwise circulation of relatively saline waters (above the 35 PSU isohaline), corresponding to the circulation in the Atlantic basin (Fig. 7c); (3) the Indo-Pacific circulation of relatively fresh waters (below the 35 PSU isohaline, Fig. 7f). The Indo-Pacific and Atlantic circulations in LGM_E are more isolated than in PD_E. Two distinct circulations are noted: (1) the Indo-Pacific circulation around the 34.5 PSU isohaline, and (2) the Atlantic circulation around the 36.5 PSU isohaline. The Southern Ocean circulation participates in linking the two different regimes existing in the Atlantic and Indo-Pacific basins.

A3 Transport in thermohaline coordinates

A3.1 Thermohaline stream function and transport of heat/freshwater in temperature and salinity coordinates

The thermohaline stream function (Eq. A8) is the volume transport brought about by the temperature and the salinity differences between the World-Ocean basins (Döös et al., 2012; Zika et al., 2012). This representation has the advantage of taking into

Title Page

Abstract

Introduction

Conclusions

References

Tables

Figures

◀

▶

◀

▶

Back

Close

Full Screen / Esc

Printer-friendly Version

Interactive Discussion



account the three-dimensional aspect of the ocean circulation. It also captures the transports and the parameters of state (temperature and salinity) of the ocean water parcels. The representation has however the disadvantage of removing the geographical coordinates.

$$5 \quad \Psi(S, \theta) = \int_{Ath(S, \theta)} (\mathbf{V} + \mathbf{V}_{eddy}) d\mathbf{A} \quad (\text{A8})$$

Here $Ath(S, \theta)$ is the part of the isothermal surface θ where the salinity is less than S , \mathbf{V} and \mathbf{V}_{eddy} are the three dimensional eulerian and eddy-induced velocities, and $d\mathbf{A}$ is the element surface on $Ath(S, \theta)$ pointing towards increasing temperature.

10 Using this representation allows to evaluate the transport of heat within specific isohaline (Eq. A9) as well as the transport of freshwater within specific isotherm (Eq. A10). These diagnostics can be applied for understanding the oceanic reorganisations under different climate conditions and for comparing or validating different model integrations. A positive heat transport is a transport towards increasing salinity and vice versa for negative transport values. Similarly, a positive freshwater transport is a transport from cold to warm waters.

$$15 \quad \mathcal{H}(S) = -\rho C_p \int_{\theta_{min}}^{\theta_{max}} \Psi(S, \theta) d\theta \quad (\text{A9})$$

Here S is the salinity, θ the temperature, $\rho = 1035 \text{ kg m}^{-3}$ the average density of seawater and $C_p = 4000 \text{ J (kg }^\circ\text{C)}^{-1}$ the specific heat for seawater, θ_{min} and θ_{max} the minimum and maximum temperature considered.

$$20 \quad \mathcal{F}(\theta) = - \int_{S_{min}}^{S_{max}} \frac{\Psi(S, \theta)}{S_r} dS \quad (\text{A10})$$

Glacial and inter-glacial THC

M. Ballarotta et al.

Title Page	
Abstract	Introduction
Conclusions	References
Tables	Figures
◀	▶
◀	▶
Back	Close
Full Screen / Esc	
Printer-friendly Version	
Interactive Discussion	



Here θ is the temperature, S is the salinity, and $S_r = 35$ PSU is a constant reference salinity, S_{\min} and S_{\max} the minimum and maximum salinity considered.

The thermohaline stream function and the associated heat and freshwater transports in LGM_E and PD_E are shown in Figs. 8 and 9.

5 **A3.2 Turnover time**

The thermohaline stream function and the volumetric distribution in the temperature-salinity diagram allow to estimate the turnover time τ (Eq. A11) in each stream layer (Döös et al., 2012). In a steady state climate, it is the ratio of the volume of sea-water (in m³) between two successive streamlines $V(\Delta\Psi)$ to the corresponding volume transport V (in Sv $\equiv 10^6$ m³ s⁻¹) between the streamlines.

$$\tau(\Delta\Psi) = \frac{V(\Delta\Psi)}{\Delta\Psi} \quad (\text{A11})$$

The turnover times for LGM_E and PD_E are shown in Figs. 12 and 13.

Supplementary material related to this article is available online at <http://www.ocean-sci-discuss.net/11/979/2014/osd-11-979-2014-supplement.pdf>.

Acknowledgements. This work has been financially supported by the Bert Bolin Centre for Climate Research and by the Swedish Research Council. The Swedish National Infrastructure for Computing (SNIC) is gratefully acknowledged for providing the computer time on the Vagn and Ekman facilities funded by the Knut and Alice Wallenberg foundation.

Title Page

Abstract

Introduction

Conclusions

References

Tables

Figures

◀

▶

◀

▶

Back

Close

Full Screen / Esc

Printer-friendly Version

Interactive Discussion



References

- Adkins, J. F. and Schrag, D. P.: Pore fluid constraints on deep ocean temperature and salinity during the Last Glacial Maximum, *Geophys. Res. Lett.*, 28, 771–774, doi:10.1029/2000GL011597, 2001. 994
- 5 Adkins, J. F., McIntyre, K., and Schrag, D. P.: The Salinity, Temperature, and $\delta^{18}\text{O}$ of the Glacial Deep Ocean, *Science*, 298, 1769–1773, doi:10.1126/science.1076252, 2002. 994
- Ballarotta, M., Brodeau, L., Brandefelt, J., Lundberg, P., and Döös, K.: Last Glacial Maximum world ocean simulations at eddy-permitting and coarse resolutions: do eddies contribute to a better consistency between models and palaeoproxies?, *Clim. Past*, 9, 2669–2686, doi:10.5194/cp-9-2669-2013, 2013. 983
- 10 Barnier, B., Madec, G., Penduff, T., Molines, J. M., Tréguier, A. M. Le Sommer, J., Beckmann, A., Biastoch, A. Böning, C., Dengg, J., Derval, C., Durand, E., Gulev, S., Remy, E., Talandier, C., Theetten, S., Maltrud, M., McClean, J., and De Cuevas, B.: Impact of partial steps and momentum advection schemes in a global ocean circulation model at eddy-permitting resolution, *Ocean Dynam.*, 56, 543–567, doi:10.1007/s10236-006-0082-1, 2006. 983
- 15 Barnier, B., Brodeau, L., LeSommer, J., Molines, J.-M., Penduff, T., Theetten, S., Tréguier, A.-M., Madec, G., Biastoch, A., Böning, C., Dengg, J., Gulev, S., Bourdallé, B. R., Chanut, J., Garric, G., Coward, A., de Cuevas, B., New, A., Haines, K., Smith, G. C., Drijfhout, S., Hazeleger, W., Severijns, C., and Myers, P.: Eddy-permitting ocean circulation hindcasts of past decades, *CLIVAR Exchanges*, 12, 8–10, 2007. 983
- 20 Bryan, F. O., Danabasoglu, G., Nakashiki, N., Yoshida, Y., Kim, D. H., Tsutsui, J., and Doney, S. C.: Response of the North Atlantic thermohaline circulation and ventilation to increasing carbon dioxide in CCSM3, *J. Climate*, 19, 2382–2397, doi:10.1175/JCLI3757.1, 2006 981
- 25 Brandefelt, J. and Otto-Bliesner, B. L.: Equilibration and variability in a Last Glacial Maximum climate simulation with CCSM3, *Geophys. Res. Lett.*, 36, 1–5, doi:10.1029/2009GL040364, 2009. 983, 991, 993
- Brodeau, L., Barnier, B., Tréguier, A. M., Penduff, T., and Gulev, S.: An ERA40-based atmospheric forcing for global ocean circulation models, *Ocean Model.*, 31, 88–104, doi:10.1016/j.ocemod.2009.10.005, 2010. 983
- 30 Broecker, W. S.: The great ocean conveyor, *Oceanography*, 4, 79–89, 1991. 981, 989

OSD

11, 979–1022, 2014

Glacial and inter-glacial THC

M. Ballarotta et al.

Title Page

Abstract

Introduction

Conclusions

References

Tables

Figures

◀

▶

◀

▶

Back

Close

Full Screen / Esc

Printer-friendly Version

Interactive Discussion



**Glacial and
inter-glacial THC**

M. Ballarotta et al.

Title Page

Abstract

Introduction

Conclusions

References

Tables

Figures

◀

▶

◀

▶

Back

Close

Full Screen / Esc

Printer-friendly Version

Interactive Discussion



- Butzin, M., Prange, M., and Lohmann, G.: Radiocarbon simulations for the glacial ocean: the effects of wind stress, Southern Ocean sea ice and Heinrich events, *Earth Planet. Sc. Lett.*, 235, 45–61, doi:10.1016/j.epsl.2005.03.003, 2005. 993
- Curry, W. B.: Glacial water mass geometry and the distribution of $\delta^{13}\text{C}$ of ΣCO_2 in the western Atlantic Ocean, *Paleoceanography*, 20, 1–13, doi:10.1029/2004PA001021, 2005.
- Döös, K. and Webb, D.: The Deacon Cell and the other meridional cells of the Southern Ocean, *J. Phys. Oceanogr.*, 24, 429–442, 1994. 982
- Döös, K., Nilsson, J., Nycander, J., Brodeau, L., and Ballarotta, M.: The World Ocean Thermohaline Circulation, *J. Phys. Oceanogr.*, 42, 1445–1460, doi:10.1175/JPO-D-11-0163.1, 2012. 982, 999, 1001
- Dufresne, J.-L., Foujols, M.-A., Denvil, S., Caubel, A., Marti, O., Aumont, O., Balkanski, Y., Bekki, S., Bellenger, H., Benshila, R., Bony, S., Bopp, L., Braconnot, P., Brockmann, P., Cadule, P., Cheruy, F., Codron, F., Cozic, A., Cugnet, D., de Noblet, N., Duvel, J.-P., Ethé, C., Fairhead, L., Fichefet, T., Flavoni, S., Friedlingstein, P., Grandpeix, J.-Y., Guez, L., Guilyardi, E., Hauglustaine, D., Hourdin, F., Idelkadi, A., Ghattas, J., Joussaume, S., Kageyama, M., Krinner, G., Labetoulle, S., Lahellec, A., Lefebvre, M.-P., Lefevre, F., Levy, C., Li, Z., Lloyd, J., Lott, F., Madec, G., Mancip, M., Marchand, M., Masson, S., Meurdesoif, Y., Mignot, J., Musat, I., Parouty, S., Polcher, J., Rio, C., Schulz, M., Swingedouw, D., Szopa, S., Talandier, C., Terray, P., Viovy, N., and Vuichard, N.: Climate change projections using the IPSL-CM5 Earth System Model: from CMIP3 to CMIP5, *Clim. Dynam.*, 40, 2123–2165, doi:10.1007/s00382-012-1636-1, 2013. 983
- Duplessy, J. C., Shackleton, N. J., and Fairbanks, R. G.: Deepwater source variations during the last climatic cycle and their impact on the global deepwater circulation, *Paleoceanography*, 3, 343–360, doi:10.1029/PA003i003p00343, 1988.
- Drijfhout, S. S.: What sets the surface eddy mass flux in the Southern Ocean?, *J. Phys. Oceanogr.*, 35, 2152–2166, 2005 992
- Drijfhout, S. S., de Vries, P., Döös, K., and Coward, A. C.: Impact of eddy-induced transport on the Lagrangian structure of the upper branch of the thermohaline circulation *J. Phys. Oceanogr.*, 33, 2141–2155, 2003 992
- Evans, H. K. and Hall, I. R.: Deepwater circulation on Blake Outer Ridge (western North Atlantic) during the Holocene, Younger Dryas, and Last Glacial Maximum, *Geochem. Geophys. Geosy.*, 9, Q03023, doi:10.1029/2007GC001771, 2008. 993

Glacial and
inter-glacial THC

M. Ballarotta et al.

Title Page

Abstract

Introduction

Conclusions

References

Tables

Figures

◀

▶

◀

▶

Back

Close

Full Screen / Esc

Printer-friendly Version

Interactive Discussion



Fichefet, T. and Morales Maqueda, M. A.: Sensitivity of a global sea ice model to the treatment of ice thermodynamics and dynamics, *J. Geophys. Res.*, 102, 12609–12646, doi:10.1029/97JC00480, 1997. 983

Ganachaud, A. and Wunsch, C.: Improved estimates of global ocean circulation, heat transport and mixing from hydrographic data, *Nature*, 408, 453–457, 2000. 981

Gent, P. R. and McWilliams, J. C.: Isopycnal mixing in ocean circulation models, *J. Phys. Oceanogr.*, 20, 150–155, doi:10.1175/1520-0485(1990)020<0150:IMIOCM>2.0.CO;2, 1990. 983

Gherardi, J. M., Labeyrie, L., Nave, S., Francois, R., McManus, J. F., and Cortijo, E.: Glacial-interglacial circulation changes inferred from $^{231}\text{Pa}/^{230}\text{Th}$ sedimentary record in the North Atlantic region, *Paleoceanography*, 24, 1–14, doi:10.1029/2008PA001696, 2009. 993

Grist, J. P., Josey, S. A., and Marsh, R.: Surface estimates of the Atlantic overturning in density space in an eddy-permitting ocean model, *J. Geophys. Res.*, 117, C06012, doi:10.1029/2011JC007752, 2012. 992

Gruber, N., Gloor, M., Mikaloff Fletcher, S. E., Doney, S. C., Dutkiewicz, S., Follows, M. J., Gerber, M., Jacobson, A. R., Joos, F., Lindsay, K., Menemenlis, D., Mouchet, A., Müller, S. A., Sarmiento, J. L., and Takahashi, T.: Oceanic sources, sinks, and transport of atmospheric CO_2 , *Global Biogeochem. Cy.*, 23, GB1005, doi:10.1029/2008GB003349, 2009. 981

Hazeleger, W.: EC-Earth: a seamless earth system prediction approach in action, *B. Am. Meteorol. Soc.*, 3, 1357–1363, doi:10.1175/2010BAMS2877.1, 2010. 983

Hesse, T., Butzin, M., Bickert, T., and Lohmann, G.: A model-data comparison of $\delta^{13}\text{C}$ in the glacial Atlantic Ocean, *Paleoceanography*, 26, PA3220, doi:10.1029/2010PA002085, 2011. 993

Hirst, A., Jackett, D., and McDougall, T.: The meridional overturning cells of a world ocean model in neutral density coordinates, *J. Phys. Oceanogr.*, 26, 775–791, 1996 982

Huang, R. X.: *Ocean Circulation – Wind-Driven and Thermohaline Processes*, WHOI, 2010.

Jackett, D. and McDougall, T. J.: Minimal adjustment of hydrostatic profiles to achieve static stability, *J. Atmos. Ocean. Tech.*, 12, 381–389, doi:10.1175/1520-0426(1995)012<0381:MAOHPT>2.0.CO;2, 2003. 983

Knight, J. R., Allan, R. J., Folland, C. K., Vellinga, M., and Mann, M. E.: Ocean ventilation and sedimentation since the glacial maximum at 3 km in the western North Atlantic, *Geochem. Geophys. Geosy.*, 3, 1–14, doi:10.1029/2001GC000283, 2002. 981

Glacial and inter-glacial THC

M. Ballarotta et al.

Title Page

Abstract

Introduction

Conclusions

References

Tables

Figures

◀

▶

◀

▶

Back

Close

Full Screen / Esc

Printer-friendly Version

Interactive Discussion



- Knight, J. R., Allan, R. J., Folland, C. K., Vellinga, M., and Mann, M. E.: A signature of persistent natural thermohaline circulation cycles in observed climate, *Geophys. Res. Lett.*, 32, L20708, doi:10.1029/2005GL024233, 2005. 981
- 5 Kuhlbrodt, T., Griesel, A., Montoya, M., Levermann, A., Hofmann, M., and Rahmstorf, S.: On the driving processes of the Atlantic meridional overturning circulation, *Rev. Geophys.*, 45, RG2001, doi:10.1029/2004RG000166, 2007.
- Labeyrie, L. D., Duplessy, J. C., Duprat, J., Juillet-Leclerc, A., Moyes, J., Michel, E., Kallel, N., and Shackleton, N. J.: Changes in the vertical structure of the north Atlantic ocean between glacial and modern times, *Quaternary Sci. Rev.*, 11, 401–413, doi:10.1016/0277-3791(92)90022-Z, 1992.
- 10 Lee, M. and Coward, A.: Eddy mass transport for the Southern Ocean in an eddy-permitting global ocean model, *Ocean Model.*, 5, 249–266, 2003 982
- Letcher, T. M.: *Climate Change: Observed Impacts on Planet Earth*, 1st Edn., Elsevier, 2009. 981
- 15 Lippold, J., Luo, Y., Francois, R., Allen, S. E., Gherardi, J., Pichat, S., Hickey, B., and Schulz, H.: Strength and geometry of the glacial Atlantic meridional overturning circulation, *Nat. Geosci.*, 5, 813–816, doi:10.1038/ngeo1608, 2012. 993
- Lynch-Stieglitz, J., Curry, W. B., and Slowey, N.: Weaker Gulf Stream in the Florida straits during the Last Glacial Maximum, *Nature*, 402, 644–648, doi:10.1038/45204, 1999. 993
- 20 Lynch-Stieglitz, J., Adkins, J. F., Curry, W. B., Dokken, T., Hall, I., Herguera, J. C., Hirschi, J., Ivanova, E., Kissel, C., Marchal, O., Marchitto, T. M., McCave, I. N., McManus, J. F., Mulitza, S., Ninnemann, U., Peeters, F., Yu, E. F., and Zahn, R.: Atlantic meridional overturning circulation during the Last Glacial Maximum, *Science*, 316, 66–69, doi:10.1126/science.1137127, 2007. 993
- 25 McDougall, T.: Neutral surfaces in the ocean: implications for modelling, *Geophys. Res. Lett.*, 14, 797–800, 1987. 982
- Madec, G.: *NEMO ocean engine*, Technical Report 27, Institut Pierre-Simon Laplace (IPSL), 2008. 983
- Manabe, S. and Stouffer, R. J.: Multiple-century response of a coupled ocean-atmosphere model to an increase of atmospheric carbon dioxide, *Science*, 7, 5–23, doi:10.1175/1520-0442(1994)007<0005:MCROAC>2.0.CO;2, 1994. 981
- 30

**Glacial and
inter-glacial THC**

M. Ballarotta et al.

Title Page

Abstract

Introduction

Conclusions

References

Tables

Figures

◀

▶

◀

▶

Back

Close

Full Screen / Esc

Printer-friendly Version

Interactive Discussion



- Marchitto, T. M. and Broecker, W. S.: Deep water mass geometry in the glacial Atlantic Ocean: a review of constraints from the paleonutrient proxy Cd/Ca, *Geochem. Geophys. Geosy.*, 7, Q12003, doi:10.1029/2006GC001323, 2006. 993
- Marshall, J. and Speer, K.: Closure of the meridional overturning circulation through Southern Ocean upwelling, *Nat. Geosci.*, 5, 171–180, doi:10.1038/ngeo1391, 2012. 981
- Martin, P. A., Lea, D. W., Rosenthal, Y., Shackleton, N. J., Sarnthein, M., and Papenfuss, T.: Quaternary deep sea temperature histories derived from benthic foraminiferal Mg/Ca, *Earth Planet. Sc. Lett.*, 198, 193–209, doi:10.1016/S0012-821X(02)00472-7, 2002. 994
- McManus, J. F., Francois, R., Gherardi, J. M., Keigwin, L. D., and Brown-Leger, S.: Collapse and rapid resumption of Atlantic meridional circulation linked to deglacial climate changes, *Nature*, 428, 834–837, doi:10.1038/nature02494, 2004.
- Otto-Bliesner, B. L., Hewitt, C. D., Marchitto, T. M., Brady, E. C., Abe-Ouchi, A., Crucifix, M., Murakami, S., and Weber, S. L.: Last Glacial Maximum ocean thermohaline circulation: PMIP2 model intercomparisons and data constraints, *Geophys. Res. Lett.*, 34 1–6, doi:10.1029/2007GL029475, 2007. 991, 993
- Rahmstorf, S.: Ocean circulation and climate during the past 120,000 years, *Nature*, 419, 207–14, doi:10.1038/nature01090, 2002. 981
- Richardson, P.: On the history of meridional overturning circulation schematic diagrams, *Progr. Oceanogr.*, 76, 466–486, doi:10.1016/j.pocean.2008.01.005, 2008. 981
- Sloyan, B. and Rintoul, S.: The Southern Ocean limb of the global deep overturning circulation, *J. Phys. Oceanogr.*, 31, 143–173, 2001. 992
- Sarnthein, M., Winn, K., Jung, S. J. A., Duplessy, J. C., Labeyrie, J. C., Erlenkeuser, H., and Ganssen, G.: Changes in East Atlantic Deepwater Circulation over the last 30,000 years: eight time slice reconstructions, *Paleoceanography*, 9, 209–267, doi:10.1029/93PA03301, 1994.
- Schmittner, A., Latif, M., and Schneider, B.: Model projections of the North Atlantic thermohaline circulation for the 21st century assessed by observations, *Geophys. Res. Lett.*, 32, L23710, doi:10.1029/2005GL024368, 2005. 981
- Storkey, D. Blockley, E. W., Furner, R., Giuavarc’h, C., Lea, D., Martin, M. J., Barciela, R. M., Hines, A., Hyder, P., and Siddorn, J. R.: Forecasting the ocean state using NEMO: the new FOAM system, *Journal of Operational Oceanography*, 3, 3–15, 2010. 983
- Tagliabue, A., Bopp, L., Roche, D. M., Bouttes, N., Dutay, J.-C., Alkama, R., Kageyama, M., Michel, E., and Paillard, D.: Quantifying the roles of ocean circulation and biogeochemistry

Glacial and inter-glacial THC

M. Ballarotta et al.

Title Page

Abstract

Introduction

Conclusions

References

Tables

Figures

◀

▶

◀

▶

Back

Close

Full Screen / Esc

Printer-friendly Version

Interactive Discussion



in governing ocean carbon-13 and atmospheric carbon dioxide at the last glacial maximum, *Clim. Past*, 5, 695–706, doi:10.5194/cp-5-695-2009, 2009. 993

Toggweiler, J. R. and Samuels, B.: On the ocean's large-scale circulation near the limit of no vertical mixing, *Journal of Operational Oceanography*, 28, 1832–1852, doi:10.1175/1520-0485(1998)028<1832:OTOSLS>2.0.CO;2, 1998. 981

Treguier, A. M., England, M. H., Rintoul, S. R., Madec, G., Le Sommer, J., and Molines, J.-M.: Southern Ocean overturning across streamlines in an eddying simulation of the Antarctic Circumpolar Current, *Ocean Sci.*, 3, 491–507, doi:10.5194/os-3-491-2007, 2007. 982

Viebahn, J. and Eden, C.: Standing eddies in the meridional overturning circulation, *J. Phys. Oceanogr.*, 42, 1486–1508, doi:10.1175/JPO-D-11-087.1, 2012. 982

Voldoire, A., Sanchez-Gomez, E., Salas y Méliá, D., Decharme, B., Cassou, C. Sénési, S., Valcke, S., Beau, I., Alias, A., Chevallier, M. Déqué, M., Deshayes, J., Douville, H., Fernandez, E., Madec, G., Maiconnave, E., Moine, M.-P., Planton, S., Saint-Martin, D., Szopa, S., Tyteca, S., Alkama, R., Belamari, S., Braun, A., Coquart, L., and Chauvin, F.: The CNRM-CM5.1 global climate model: description and basic evaluation, *Clim. Dynam.*, 40, 2091–2121, doi:10.1007/s00382-011-1259-y, 2012. 983

Weber, S. L., Drijfhout, S. S., Abe-Ouchi, A., Crucifix, M., Eby, M., Ganopolski, A., Murakami, S., Otto-Bliesner, B., and Peltier, W. R.: The modern and glacial overturning circulation in the Atlantic ocean in PMIP coupled model simulations, *Clim. Past*, 3, 51–64, doi:10.5194/cp-3-51-2007, 2007. 991

Wunsch, C.: What is the thermohaline circulation?, *Science*, 298, 1179–81, doi:10.1126/science.1079329, 2002.

Yu, E. F., Francois, R., and Bacon, M. P.: Similar rates of modern and last-glacial ocean thermohaline circulation inferred from radiochemical data, *Nature*, 379, 689–694, doi:10.1038/379689a0, 1996. 993

Zhang, R.: Latitudinal dependence of Atlantic meridional overturning circulation (AMOC) variations, *Geophys. Res. Lett.*, 37, L16703, doi:10.1029/2010GL044474, 2010. 992

Zhang, R., Delworth, T. L., and Held, I. M.: Can the Atlantic Ocean drive the observed multidecadal variability in Northern Hemisphere mean temperature?, *Geophys. Res. Lett.*, 34, L02709, doi:10.1029/2006GL028683, 2007. 981

Zhang, X., Lohmann, G., Knorr, G., and Xu, X.: Different ocean states and transient characteristics in Last Glacial Maximum simulations and implications for deglaciation, *Clim. Past*, 9, 2319–2333, doi:10.5194/cp-9-2319-2013, 2013. 992, 993

Zickfeld, K., Eby, M., and Weaver, A. J.: Carbon-cycle feedbacks of changes in the Atlantic meridional overturning circulation under future atmospheric CO₂, *Global Biogeochem. Cy.*, 22, 1–14, doi:10.1029/2007GB003118, 2008. 981

5 Zika, J. D., England, M. H., and Sijp, W. P.: The ocean circulation in thermohaline coordinates, *J. Phys. Oceanogr.*, 42, 708–724, doi:10.1175/JPO-D-11-0139.1, 2012. 982, 999

Glacial and inter-glacial THC

M. Ballarotta et al.

Title Page

Abstract

Introduction

Conclusions

References

Tables

Figures

◀

▶

◀

▶

Back

Close

Full Screen / Esc

Printer-friendly Version

Interactive Discussion



Glacial and inter-glacial THC

M. Ballarotta et al.

Table 1. Maximum volume transport in the LGM_E and PD_E simulations in the tropical cells, the AMOC cell, the Deacon Cell, the deep cell representative of the AABW (in the Atlantic basin and the global ocean) and the Conveyor Belt cell for the different coordinates frameworks

	$\Psi(y, z)^{\max}$		$\Psi(y, \gamma)^{\max}$		$\Psi(y, \theta)^{\max}$		$\Psi(y, S)^{\max}$		$\Psi(S, \theta)^{\max}$	
	LGM _E	PD _E	LGM _E	PD _E	LGM _E	PD _E	LGM _E	PD _E	LGM _E	PD _E
Tropical cell	≈ 35 Sv	≈ 35 Sv	≈ 30 Sv	≈ 27 Sv	≈ 30 Sv	≈ 26 Sv	≈ 20 Sv	≈ 20 Sv	24 Sv	21 Sv
AMOC	13 Sv	13 Sv	9 Sv	13 Sv	16 Sv	19 Sv	10 Sv	12 Sv		
Deacon cell/Residual cell	28 Sv	24 Sv	13 Sv	13 Sv	4 Sv	8 Sv	29 Sv	30 Sv		
Deep cell	19 Sv	8 Sv	12 Sv	16 Sv	41 Sv	44 Sv	10 Sv	18 Sv		
Deep cell (in Atlantic basin)	2 Sv	2 Sv	2 Sv	2 Sv	2 Sv	4 Sv	17 Sv	6 Sv		
Conveyor Belt cell									20 Sv	23 Sv

[Title Page](#)
[Abstract](#)
[Introduction](#)
[Conclusions](#)
[References](#)
[Tables](#)
[Figures](#)
[◀](#)
[▶](#)
[◀](#)
[▶](#)
[Back](#)
[Close](#)
[Full Screen / Esc](#)
[Printer-friendly Version](#)
[Interactive Discussion](#)

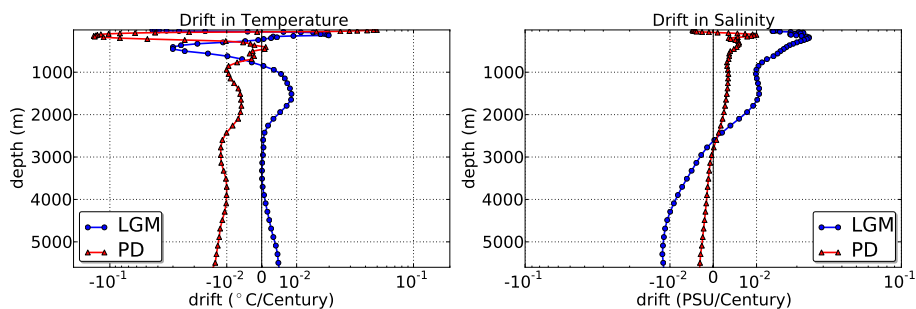



Fig. 1. Globally averaged temperature and salinity trends in final stage of the the LGM and PD simulations.

[Title Page](#)
[Abstract](#)
[Introduction](#)
[Conclusions](#)
[References](#)
[Tables](#)
[Figures](#)
[◀](#)
[▶](#)
[◀](#)
[▶](#)
[Back](#)
[Close](#)
[Full Screen / Esc](#)
[Printer-friendly Version](#)
[Interactive Discussion](#)


Glacial and inter-glacial THC

M. Ballarotta et al.

Title Page

Abstract

Introduction

Conclusions

References

Tables

Figures

◀

▶

◀

▶

Back

Close

Full Screen / Esc

Printer-friendly Version

Interactive Discussion

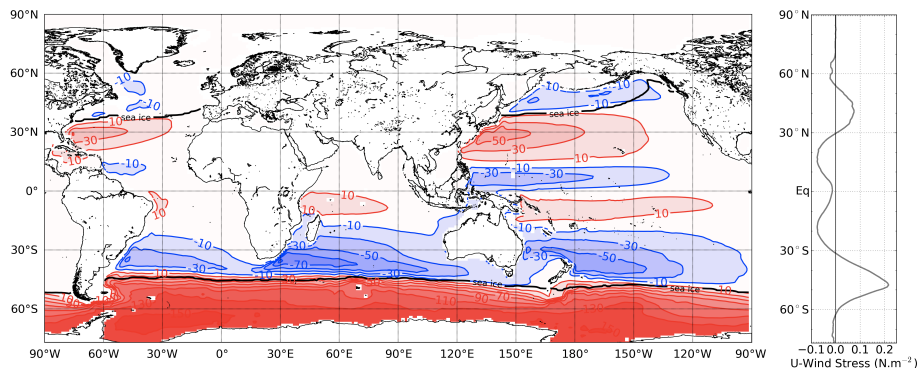


Fig. 2. Barotropic stream function for the LGM simulation. The contour interval for the circulation is 20 Sv. Red contours indicate clockwise circulations and blue contours are for anti-clockwise circulations. The thick black line corresponds to the maximum sea-ice extent. Left diagram shows the time and zonally averaged zonal-wind-stress over the ocean.

Glacial and inter-glacial THC

M. Ballarotta et al.

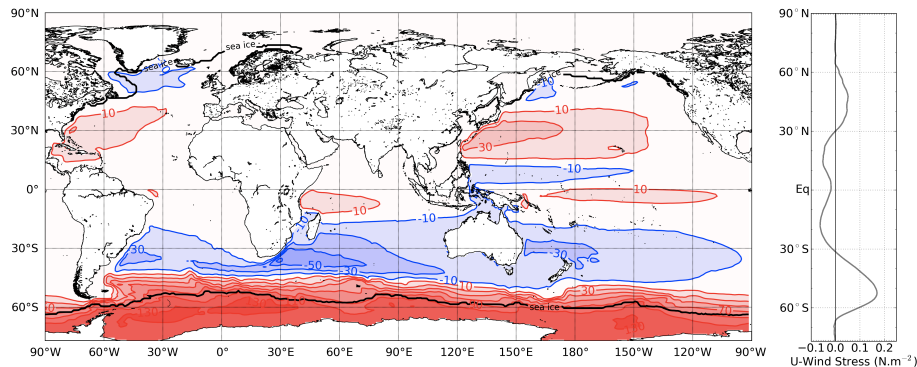


Fig. 3. Barotropic stream function for the PD simulation. The contour interval for the circulation is 20 Sv. Red contours indicate clockwise circulations and blue contours are for anti-clockwise circulations. The thick black line corresponds to the maximum sea-ice extent. Left diagram shows the time and zonally averaged zonal-wind-stress over the ocean.

[Title Page](#)[Abstract](#)[Introduction](#)[Conclusions](#)[References](#)[Tables](#)[Figures](#)[◀](#)[▶](#)[◀](#)[▶](#)[Back](#)[Close](#)[Full Screen / Esc](#)[Printer-friendly Version](#)[Interactive Discussion](#)

Title Page

Abstract

Introduction

Conclusions

References

Tables

Figures

◀

▶

◀

▶

Back

Close

Full Screen / Esc

Printer-friendly Version

Interactive Discussion

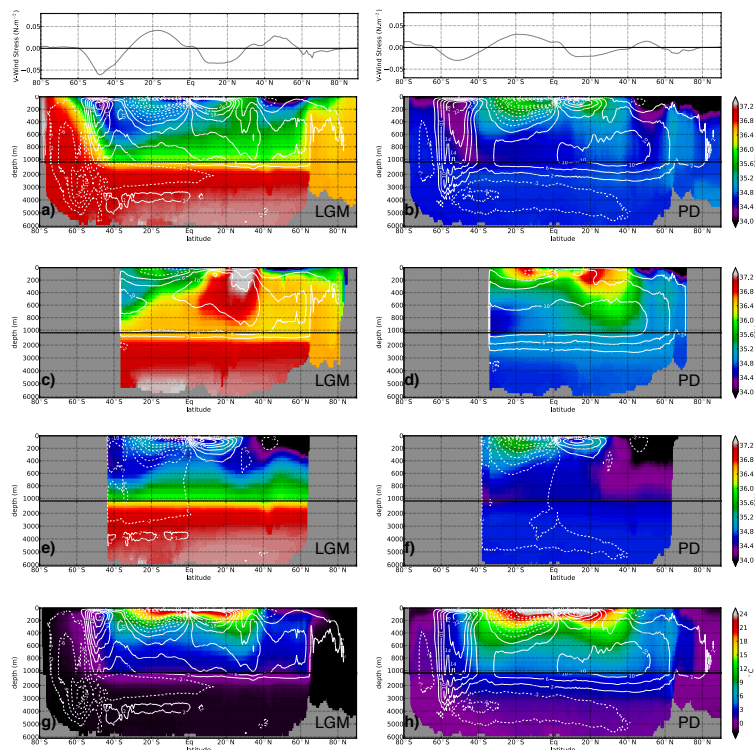


Fig. 4. LGM and PD meridional overturning circulation in depth coordinate superimposed on the temporally and zonally averaged salinity in the Global Ocean, the Atlantic basin and the Indo-Pacific basin. The contour interval for the circulation is 4 Sv. Thick lines correspond to clockwise circulations whereas dashed lines are for counter-clockwise motions. Upper diagrams show the temporally and zonally averaged meridional-wind-stress over the ocean.

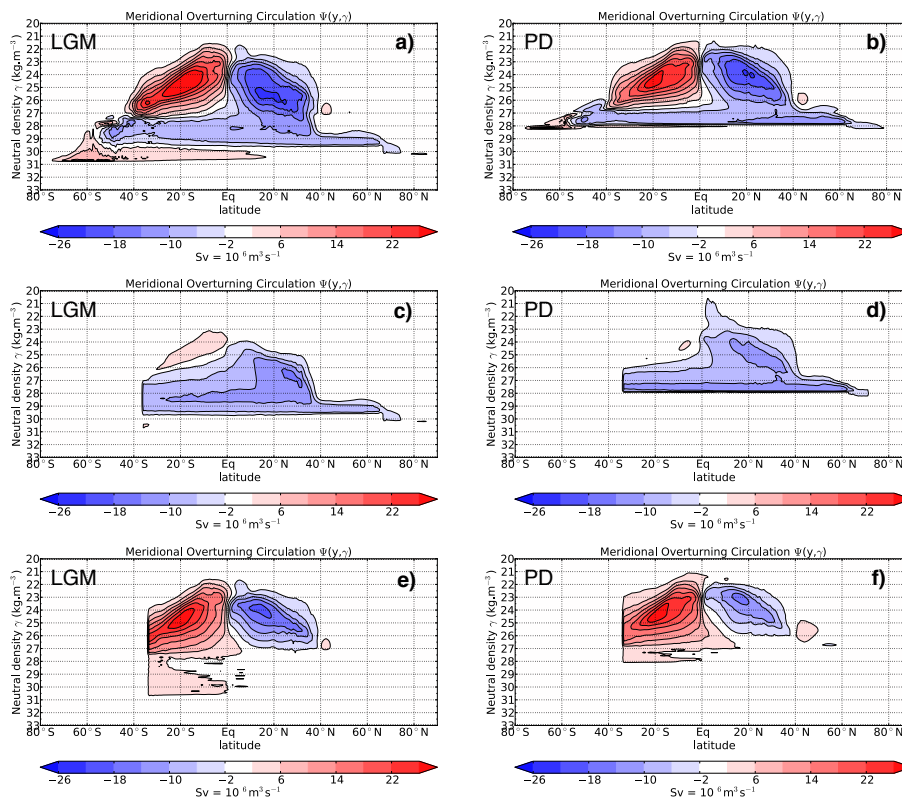


Fig. 5. LGM and PD meridional overturning circulation in neutral density coordinate for (a, b) the Global Ocean, (c, d) the Atlantic basin, and (e, f) the Indo-Pacific basin. The contour interval for the circulation is 4 Sv. The blue cells correspond to clockwise circulations whereas the red cells are for counter-clockwise motions.

Title Page

Abstract

Introduction

Conclusions

References

Tables

Figures

◀

▶

◀

▶

Back

Close

Full Screen / Esc

Printer-friendly Version

Interactive Discussion



Glacial and inter-glacial THC

M. Ballarotta et al.

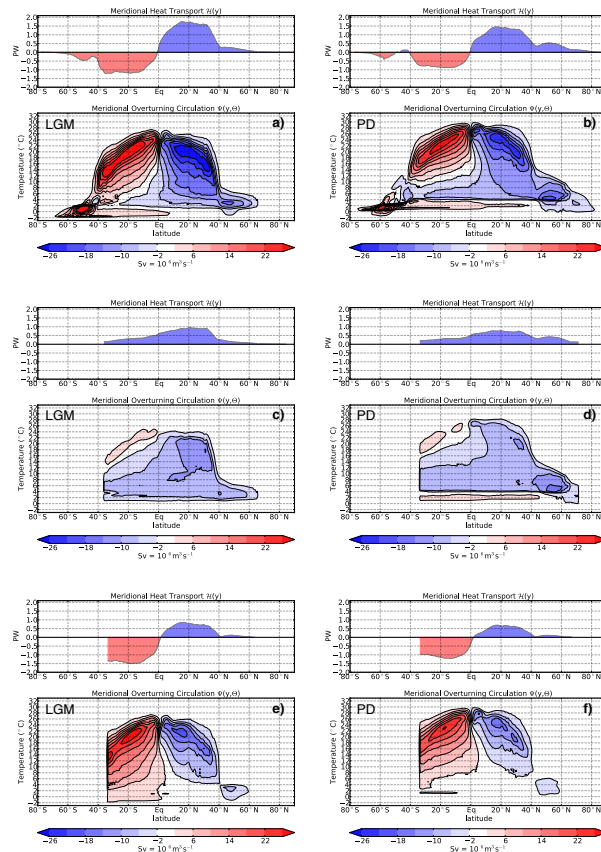


Fig. 6. LGM and PD meridional overturning circulation in temperature coordinate for **(a, b)** the Global Ocean, **(c, d)** the Atlantic basin, and **(e, f)** the Indo-Pacific basin. The contour interval for the circulation is 4 Sv. The blue cells correspond to clockwise circulations whereas the red cells are for counter-clockwise motions. For each basin, the oceanic meridional heat transport in PW is represented.

Glacial and inter-glacial THC

M. Ballarotta et al.

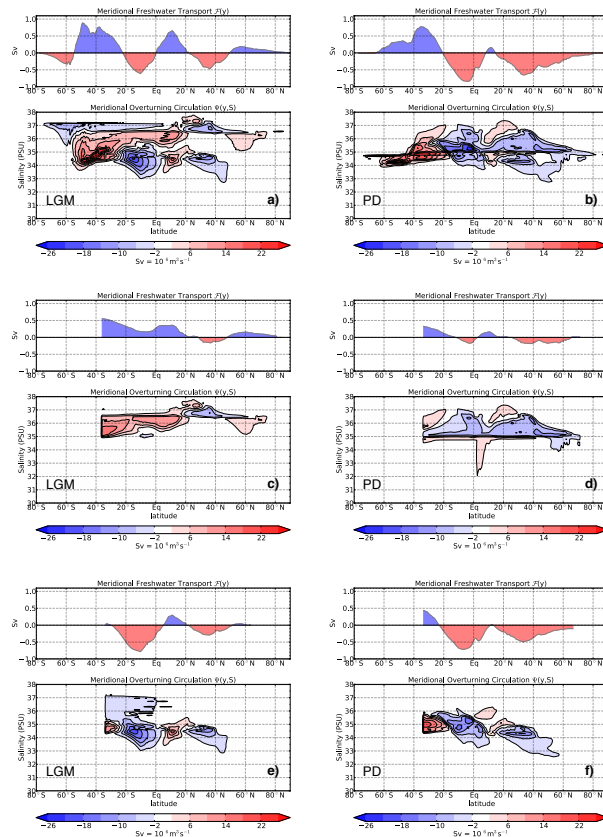


Fig. 7. LGM and PD meridional overturning circulation in salinity coordinate. The contour interval for the circulation is 4 Sv. The blue cells correspond to clockwise circulations whereas the red cells are for counter-clockwise motions. For each basin, the oceanic meridional freshwater transport in Sv is represented.

Title Page

Abstract

Introduction

Conclusions

References

Tables

Figures

◀

▶

◀

▶

Back

Close

Full Screen / Esc

Printer-friendly Version

Interactive Discussion



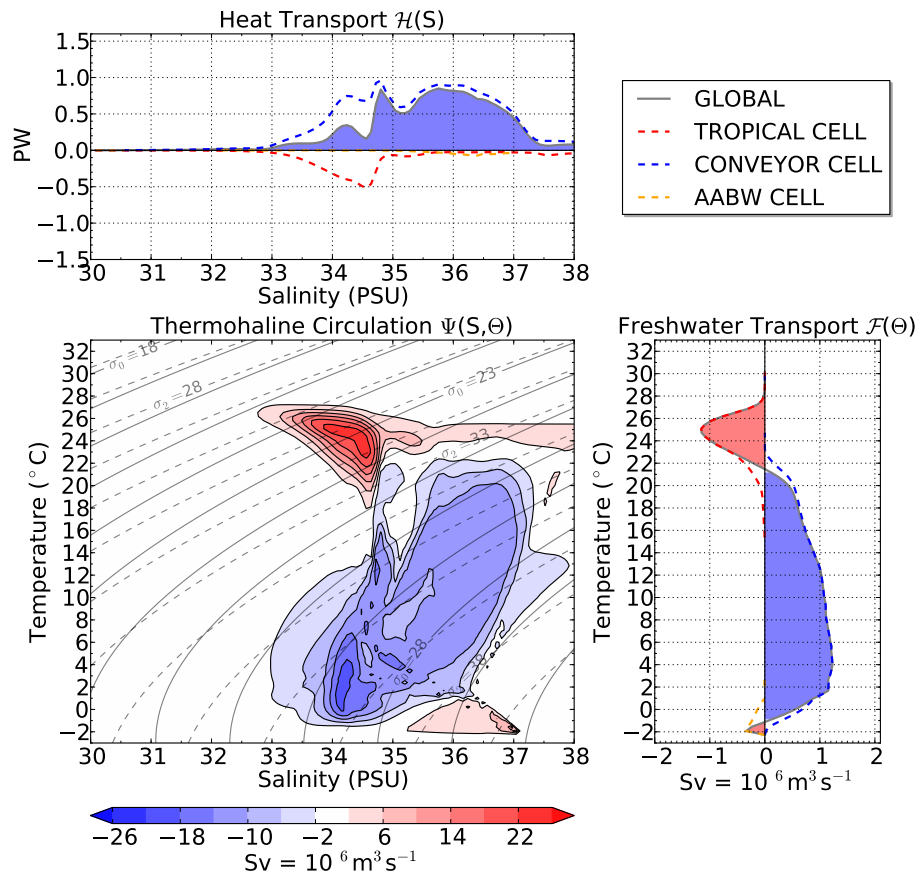


Fig. 8. LGM thermohaline stream function. The contour interval for the circulation is 4 Sv. The blue cells correspond to clockwise circulations whereas the red cells are for counter-clockwise motions. The upper diagram correspond to the oceanic heat transport within each isohaline is plotted. The left diagram shows the freshwater transport within each isotherm.

Glacial and inter-glacial THC

M. Ballarotta et al.

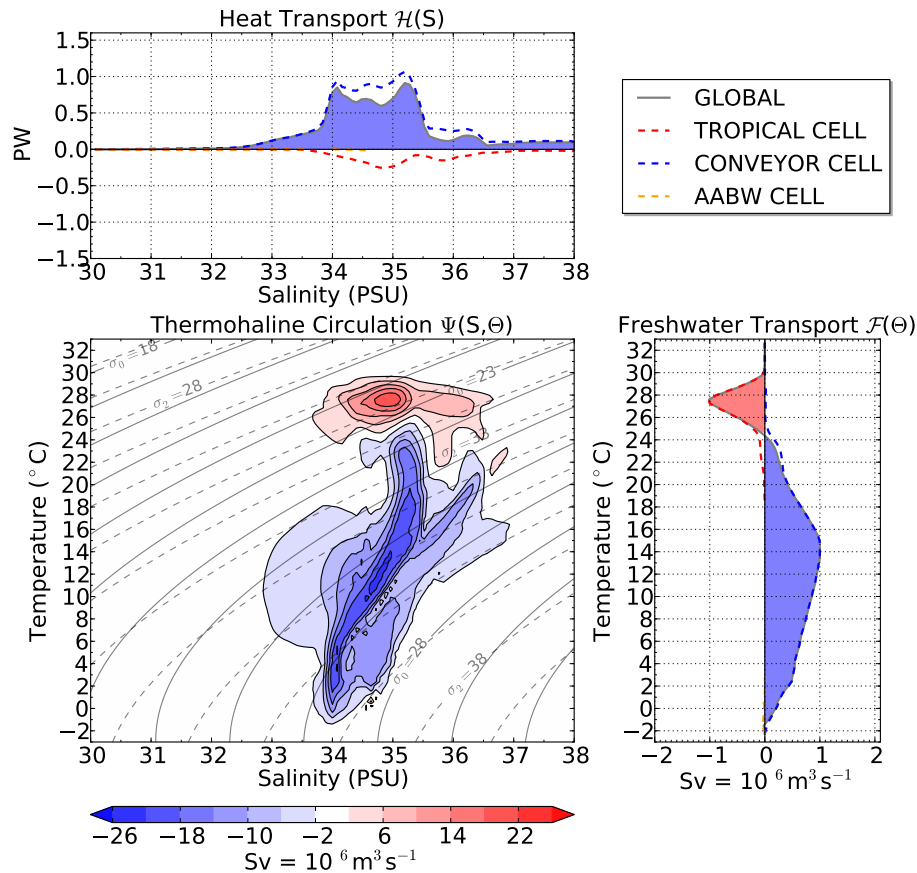


Fig. 9. PD thermohaline stream function. The contour interval for the circulation is 4 Sv. The blue cells correspond to clockwise circulations whereas the red cells are for counter-clockwise motions. The upper diagram correspond to the oceanic heat transport within each isohaline is plotted. The left diagram shows the freshwater transport within each isotherm.

Glacial and
inter-glacial THC

M. Ballarotta et al.

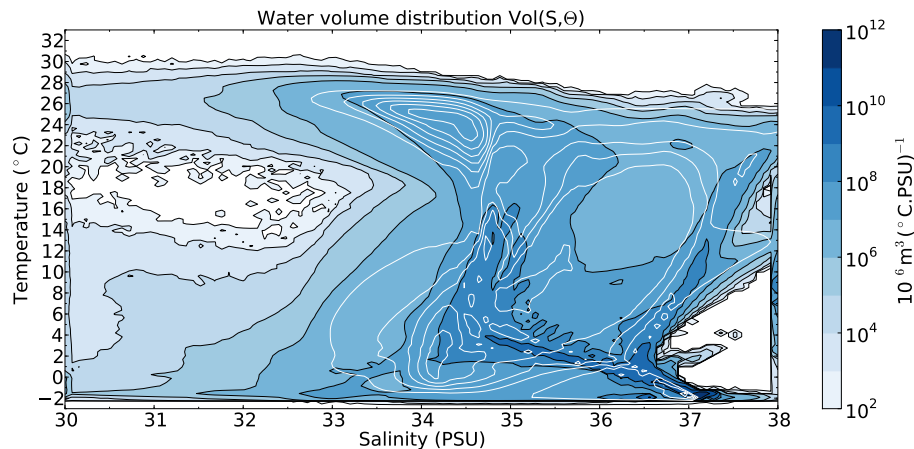


Fig. 10. Sea-water volumetric distribution projected in the temperature-salinity diagram for the LGM simulation. The LGM thermohaline stream function is superimposed. The contour interval for the volume is $10^7 \text{ m}^{-3} (\text{°C.PSU})^{-1}$.

Title Page

Abstract

Introduction

Conclusions

References

Tables

Figures

◀

▶

◀

▶

Back

Close

Full Screen / Esc

Printer-friendly Version

Interactive Discussion



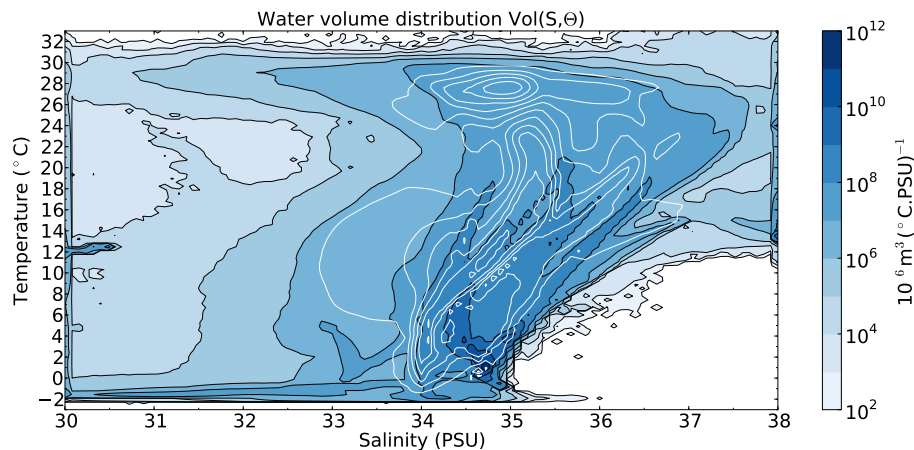


Fig. 11. Sea-water volumetric distribution projected in the temperature-salinity diagram for the PD simulation. The PD thermohaline stream function is superimposed. The contour interval for the volume is $10^7 \text{ m}^{-3} (\text{°C.PSU})^{-1}$.

[Title Page](#)[Abstract](#)[Introduction](#)[Conclusions](#)[References](#)[Tables](#)[Figures](#)[◀](#)[▶](#)[◀](#)[▶](#)[Back](#)[Close](#)[Full Screen / Esc](#)[Printer-friendly Version](#)[Interactive Discussion](#)

Glacial and
inter-glacial THC

M. Ballarotta et al.

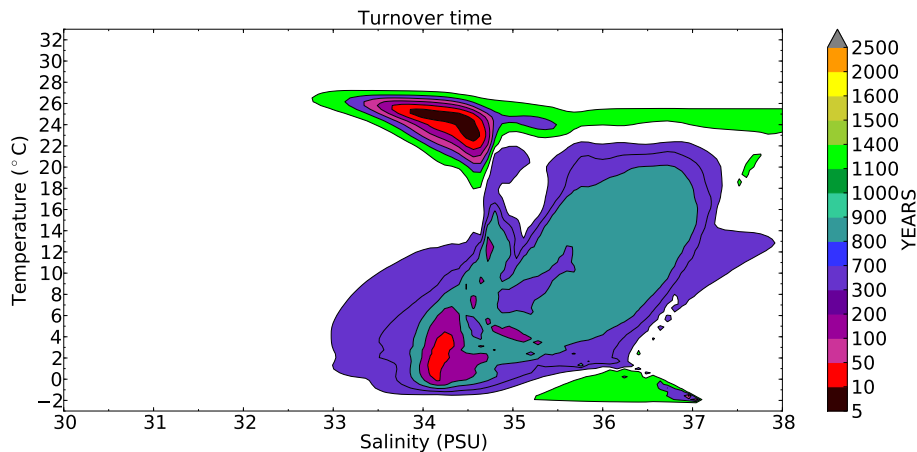


Fig. 12. Turnover times (in years) in each stream layer of the thermohaline stream function computed for the LGM experiment.

[Title Page](#)[Abstract](#)[Introduction](#)[Conclusions](#)[References](#)[Tables](#)[Figures](#)[◀](#)[▶](#)[◀](#)[▶](#)[Back](#)[Close](#)[Full Screen / Esc](#)[Printer-friendly Version](#)[Interactive Discussion](#)

Glacial and
inter-glacial THC

M. Ballarotta et al.

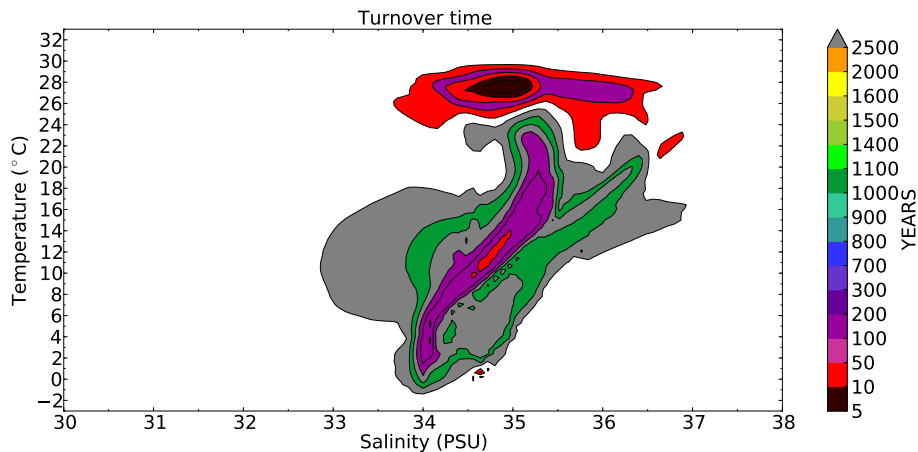


Fig. 13. Turnover times (in years) in each stream layer of the thermohaline stream function computed for the PD experiment.

[Title Page](#)[Abstract](#)[Introduction](#)[Conclusions](#)[References](#)[Tables](#)[Figures](#)[◀](#)[▶](#)[◀](#)[▶](#)[Back](#)[Close](#)[Full Screen / Esc](#)[Printer-friendly Version](#)[Interactive Discussion](#)